Histol Histopathol (2024) 39: 511-523

Histology and Histopathology
From Cell Biology to Tissue Engineering

ORIGINAL ARTICLE Open Access

E2F1-EP300 co-activator complex potentiates immune escape in nasopharyngeal carcinoma through the mediation of MELK

Qiang Wang, Qi Yu and Yueyang Liu

Otolaryngology and Head and Neck Center, Cancer Center, Department of Otolaryngology, Zhejiang Provincial People's Hospital, Affiliated People's Hospital, Hangzhou Medical College, Hangzhou, Zhejiang, PR China

Summary. Background. Nasopharyngeal carcinoma (NPC) is characterized by a highly suppressive microenvironment that protects tumor cells against immune attack and facilitates tumor progression. MELK is upregulated in various tumors, whereas its function in the immune escape remains largely unknown. In this study, we investigated the role of MELK during immune escape in NPC.

Methods. Differentially expressed genes were filtered using GEO datasets and PPI network analysis. NPC cell colony formation and motility were examined, and the impact of $CD8^+$ T cells on NPC cells was evaluated. A xenograft model was constructed to detect the growth of tumor cells and the T-cell phenotype of tumor infiltration. ChIP-qPCR and dual-luciferase assays were used to verify the transcriptional regulation of MELK by EP300/E2F1.

Findings. MELK was overexpressed in NPC, and sh-MELK suppressed the clonogenic ability, migration, and invasion of NPC cells and promoted the killing effects of $CD8^+$ T cells. These *in vitro* findings were reproduced *in vivo*. EP300 synergized E2F1 to regulate the transcription of MELK in NPC cells. Loss of EP300 or E2F1 reverted the malignant phenotype of NPC cells and promoted the immune effect of $CD8^+$ T cells. MELK further suppressed the immune effect of $CD8^+$ T cells in the presence of sh-E2F1.

Interpretation. EP300 coordinated with E2F1 to promote the transcription of MELK which promoted the growth of NPC cells and repressed the killing effect of $CD8^+$ T cells. Blockage of MELK may be a potential way to suppress the immune escape of NPC cells.

Corresponding Author: Yueyang Liu, Otolaryngology and Head and Neck Center, Cancer Center, Department of Otolaryngology, Zhejiang Provincial People's Hospital, Affiliated People's Hospital, Hangzhou Medical College, No. 158, Shangtang Road, Hangzhou 310014, Zhejiang, PR China. e-mail: liuyy_823@163.com
www.hh.um.es. DOI: 10.14670/HH-18-662

Key words: MELK, EP300, E2F1, Nasopharyngeal carcinoma, Immune escape

Introduction

According to the global cancer statistics in 2020, more than 75% of nasopharyngeal carcinoma (NPC) cases were diagnosed in East and Southeast Asia, particularly in southern China (Sung et al., 2021). NPC is an epithelial carcinoma arising from the nasopharyngeal mucosal lining among human head and neck carcinomas (HNSC), and a combination of genetic, ethnic, and environmental factors might affect its pathogenesis (Chen et al., 2019). Current therapeutic decisions are mainly made on disease stage, and the consensus is to treat stage I disease with radiotherapy alone, stage II disease with radiotherapy with or without concurrent chemotherapy, and stage III to IVB NPC with concurrent chemotherapy (Lee et al., 2015). However, recurrent and metastatic NPC is ineffective with those treatments, and the mechanisms behind are still unclear.

NPC is frequently infiltrated with different stromal cells, which makes the tumor microenvironment (TME) a highly heterogeneous harbor and protects tumor cells from immune attack (Gong et al., 2021). The development of malignant tumors requires interaction with other cells in the TME, including T cells, B cells, macrophages, dendritic cells, and natural killer cells (Xiao and Yu, 2021). In NPC, the percentage of $CD8^+$ T cells was found to be significantly higher than in normal tissues, and its expression was closely related to the recurrence and metastasis of NPC (Li et al., 2022). Programmed death-ligand 1 (PD-L1) represents an immune-checkpoint molecule that regulates type 1 T helper immune responses and mediates cancer immune evasion which is expressed on both tumor cells and/or tumor-infiltrating immune cells (Chan et al., 2017). Because NPC is characterized by immune escape in the context of a hot tumor, there is probably a wide margin

for the use of immune modulators (Baloche et al., 2020).

In this study, we predicted differentially expressed genes in NPC by comparing two datasets in the GEO database: GSE12452 and GSE13597, followed by protein-protein interaction (PPI) network construction. Maternal embryonic leucine zipper kinase (MELK) was thus identified as a hub protein. MELK belongs to the AMP-related serine-threonine kinase family, which has been implicated in many biological processes, including cell proliferation, cell death, as well as metabolism (Thangaraj et al., 2020). Knockdown of MELK has been reported to inhibit cell proliferation and epithelial-mesenchymal transition of oral squamous cell carcinoma cells *in vitro* and tumor growth *in vivo* (Li et al., 2021). Notably, MELK expression was related to cell proliferation, immune response, and neoadjuvant chemotherapy in breast cancer (Oshi et al., 2021). Nevertheless, the effects of MELK on immune escape in NPC have not been established and are expected to be probed. Here, we investigated the function and underlying mechanism of MELK in NPC.

Materials and methods

Bioinformatics prediction

Total RNA microarrays of NPC-related datasets GSE12452 and GSE13597 in the GEO database were used to analyze differentially expressed genes, setting a threshold of $p<0.05$ and $|\log2FC|>1.5$. The string database (https://cn.string-db.org/cgi/input?sessionId=bBVmVg4qX6PG&input_page_active_form=single_identifier) was used to analyze the PPI network. The GEPIA database (http://gepia.cancer-pku.cn/detail.php) was queried to analyze the expression of MELK in HNSC and the correlation of its expression with PD-L1 expression in HNSC. The hTFtarget database (http://bioinfo.life.hust.edu.cn/hTFtarget/#!/) was used to predict whether EP300 and E2F1 can regulate MELK transcription. The ChIP-seq database (http://cistrome.org/db/#/) and the UCSC Genome Browser (http://genome.ucsc.edu/index.html) were used to analyze the binding of EP300 and E2F1 at the MELK promoter.

Cell culture and infection

Human normal nasopharyngeal epithelial cells NP69 were purchased from BeNa Culture Collection (Henan, China), and NPC cells HNE3 and C666-1 were purchased from Shanghai Chuan Qiu Biotechnology Co., Ltd. (Shanghai, China). Cells were cultured in Dulbecco's modified Eagle's medium containing 10% FBS at 37°C in an incubator with 5% CO_2. $CD8^+$ T cells (ATCC, Manassas, VA, USA) were resuscitated with 1640 medium and activated and amplified with CD3/CD28 magnetic beads (MBS-C001, ACROBiosystems Group, Beijing, China).

The lentivirus sh-MELK (1#, 2#, 3#), sh-EP300 (1#, 2#, 3#), sh-E2F1 (1#, 2#, 3#), oe-MELK and its negative controls sh-NC or oe-NC were purchased from VectorBuilder (Guangzhou, Guangdong, China). Briefly, NPC cells were seeded into cell culture flasks and infected by adding lentivirus solution when the cells reached 70% confluence. Screening of lentivirus-infected cells was performed by adding the appropriate antibiotics 48h after infection.

RNA extraction, cDNA synthesis, and RT-qPCR

TRIzol (15596026, Invitrogen Inc., Carlsbad, CA, USA) was used for total RNA extraction, followed by quantitative analysis using SuperScript IV one-step RT-PCR (12594100, Invitrogen). The transcript level of mRNAs was normalized by comparison with the mRNA of GAPDH and was calculated using the $2^{-\Delta\Delta Ct}$ method. Specific primers were used for MELK: forward 5'-TCCTGTGGACAAGCCAGTGCTA-3' and reverse 5'-GGGAGTAGCAGCACCTGTTGAT-3'; EP300: forward 5'-GATGACCCTTCCCAGCCTCAAA-3' and reverse 5'-GCCAGATGATCTCATGGTGAAGG-3'; E2F1: forward 5'-GGACCTGGAAACTGACCATCAG-3' and reverse 5'-CAGTGAGGTCTCATAGCGTGAC-3'; GAPDH: forward 5'-GTCTCCTCTGACTTCAACAGCG-3' and reverse 5'-ACCACCCTGTTGCTGTAGCCAA-3'.

Colony formation assay

NPC cells (1000 cells/well) were plated into 6-well plates and cultured in a 5% CO_2 cell culture incubator at 37°C for 14 d. The cells were fixed with paraformaldehyde for 20 min, followed by staining with crystal violet solution (R23273, Saint-Bio, Shanghai, China). Finally, the number of colonies formed was observed and counted under the microscope.

Transwell assays

Migration and invasion of NPC cells were detected using Transwell plates. For the assay of cell invasiveness, the apical chamber was pre-coated with Matrigel. Then, the apical chamber was filled with 1×10^5 cells resuspended in a serum-free medium, and the basolateral chamber was filled with complete medium containing serum. Incubation was continued for 24h at 37°C in a 5% CO_2 cell incubator. Migrated and invaded cells in the basolateral chamber were fixed with paraformaldehyde, stained with crystal violet, and counted.

Western blot

Total protein extraction was performed with Total Protein Extraction Cell Lysis Buffer (R0278, Sigma-Aldrich Chemical Company, St Louis, MO, USA), and total protein was quantified with BCA Protein Quantification Kit (BCA1, Sigma-Aldrich). The total

protein was then separated by SDS-PAGE. The proteins on the SDS-PAGE gel were transferred to the PVDF membrane. PVDF membranes were sealed with 3% skim milk for 45 min and incubated with the corresponding primary antibodies overnight at 4°C. On the second day, PVDF membranes were incubated for 60 min at room temperature with HRP-coupled secondary antibody (ab6721, Abcam, Cambridge, UK). Immunoblots were visualized by the ECL developer. The primary antibodies used were anti-PD-L1 (1:500, 28076-1-AP, ProteinTech Group, Chicago, IL, USA), EP300 (1:1000, ab275378, Abcam), E2F1 (1:3000, ab245308, Abcam), and GAPDH (1:2000, 80570-1-RR, ProteinTech).

T cell-mediated tumor cell killing assay

$CD8^+$ T cells activated by CD3/CD28 magnetic beads were co-cultured with tumor cells in a 10:1 ratio in the cell culture plate, and the co-culture supernatant and tumor cells were harvested after 48h of co-culture. Flow cytometry analysis of tumor cell apoptosis and ELISA of Perforin and Granzyme B release from co-culture supernatants were conducted to assess the killing effect of $CD8^+$ T cells on tumor cells.

Cell apoptosis assay

Annexin V-FITC/PI Dual-stained Apoptosis Assay Kit (BB-4101, Bestbio, Shanghai, China) was used for the determination of apoptosis. NPC cells were collected, and 1×10^5 cells were resuspended with 100 μL of Annexin V conjugate. The cells were incubated with Annexin V-FITC staining solution for 15 min at 4°C and with PI staining solution for 5 min (both in the dark). Finally, the apoptosis of the cells was detected on the flow cytometer.

ELISA

Kits for Perforin (BMS2306TEN, Invitrogen), Granzyme B (DY2906-05, R&D Systems, Minneapolis, MN, USA), IL-2 (QK202, R&D system), IFN-γ (DIF50C, R&D system), and TNF-α (E-EL-H0109c, Elabscience Biotechnology Co., Ltd., Wuhan, Hubei, China) were used to detect their levels in cell culture supernatants. Briefly, the co-culture medium was centrifuged at 1000 g for 10 min at 4°C, and the supernatant (100 μL) to be tested was added to the plate which was sealed with sealing film and incubated at 37°C for 1.5h. After that, 100 μL of biotinylated detection antibody was added, and the plate was sealed and incubated at 37°C for 1h. After a 0.5h incubation with 100 μL of enzyme conjugate working solution at 37°C, the plate was incubated with 100 μL of TMB chromogenic substrate at 37°C for 15 min. Following the addition of 50 μL of termination solution, the optical density (OD) at 450 nm was read using a microplate reader. The standard curve was plotted by the concentration of the standard and the sample, and the cytokine concentration was determined from the standard curve.

Chromatin immunoprecipitation (ChIP)

EZ-Magna ChIP® A-ChIP Kit (17-408, Sigma-Aldrich) was used to determine the enrichment of MELK promoter sequences on EP300, E2F1, and H3K27Ac in NPC cells. Briefly, NPC cells were treated with formaldehyde for 15 min to cross-link proteins and DNA. Glycine was then used to inhibit the effect of formaldehyde on cells. The cells were lysed by lysis buffer and then treated with ultrasound to shear DNA. DNA was then used for immunoprecipitation with antibodies specifically targeting EP300 (1:200, ab275378, Abcam), E2F1 (1:100, ab245308, Abcam), H3K27Ac (1:100, 07-360, Sigma) or isotype control rabbit IgG overnight at 4°C. After eluting the protein and DNA complexes, the DNA was de-crosslinked with proteinase K. Finally, DNA was enriched by qPCR after purification to detect the MELK promoter on each protein.

Reporter gene assay

The wild-type (WT) MELK promoter sequence containing the binding site and the mutant (MUT) MELK promoter sequence with the binding site mutation was inserted into the PGL3-Basic vector to construct the luciferase reporter gene vectors. HEK293T cells were plated into 96-well plates, and the cells were co-transfected with liposomal transfection reagent (40802ES02, Yeasen, Shanghai, China) with the overexpression plasmid oe-EP300, shRNA plasmid sh-E2F1 or its negative controls when the cells reached 70% confluence. The luciferase activity was measured 48 h after transfection with a dual luciferase reporter gene assay kit (11402ES60, Yeasen).

Xenograft in vivo analysis

The *in vivo* assays were done according to the institutional guidelines and approved by the Animal Ethics Committee of Zhejiang Provincial People's Hospital. Ten C57BL/6 mice were purchased from Bestest (Zhuhai, Guangdong, China). HNE3 cells (5×10^6) were injected subcutaneously into the abdomen to construct a xenograft model (n=5). The long and short diameters of the tumors were measured every 5 days with vernier calipers, and the volume size of the tumor was calculated based on $V = 1/2 \times \text{long diameter} \times \text{short diameter}^2$. The mice were euthanized by intraperitoneal injection of sodium pentobarbital (150 mg/kg) 1 month after injection, and tumor tissues were collected and weighed.

Flow cytometry detection of T-cell phenotypes

Single-cell suspensions of tumor tissues were

prepared by the Tumor Dissociation Kit (130-096-730, Miltenyi Biotec Inc., Auburn, CA, USA). Subsequent screening of lymphocytes was performed with mouse $CD3^+$ magnetic beads (8802-6840-74, Invitrogen). The lymphocytes were then stained with CD8-APC (17-0081-82, Invitrogen), CD3-PE (12-0031-82, Invitrogen), IFN-γ-FITC (11-7311-41, Invitrogen), CD4-APC (17-0042-82, Invitrogen), FOXP3-PE (ab210231, Abcam), CD25-FITC (ab210332, Abcam). Finally, the percentage of $CD8^+/CD3^+$ T cells, IFN-$\gamma^+/CD8^+$ T cells, $CD3^+/CD4^+$ T cells, and $CD25^+/FOXP3^+$ (Treg cells) were detected on the flow cytometer.

Statistical analysis

Data are expressed as mean±SD. We performed a minimum of three independent experiments. Means between two groups were compared by unpaired t-test, and multiple comparisons were made by one-way or two-way analysis of variance (ANOVA) followed by all pairwise Tukey's post hoc test. Analysis was carried out using GraphPad Prism software 8.0 (GraphPad, San Diego, CA, USA). A p-value less than 0.05 was considered significant.

Results

MELK is highly expressed in NPC

We selected NPC-related datasets GSE12452 (total RNA extracted from laser-captured epithelium from 31 NPC patients and 10 normal healthy nasopharyngeal tissue specimens) and GSE13597 (snap frozen nasopharyngeal biopsies from 25 patients with histologically confirmed undifferentiated NPC and 3 patients with no evidence of malignancy) from the GEO database for the analysis of total RNA microarrays (Fig. 1A). The genes that were significantly differentially expressed in the two datasets were screened and intersected to obtain 97 intersecting genes (Fig. 1B). We performed a functional clustering analysis of the protein functions of the intersecting genes in String where MELK interacts with multiple proteins (Fig. 1C). We queried at GEPIA and found a significant increase in MELK expression in HNSC (Fig. 1D). Consistently, RT-qPCR showed that MELK was overexpressed in HNE3 cells (1.75±0.11) and C666-1 (1.53±0.14) relative to human normal nasopharyngeal epithelial cells NP69 (Fig. 1E).

MELK downregulation reverts the malignant phenotype NPC cells and lowers the expression of PD-L1

To examine the correlation between MELK expression and NPC progression, we constructed NPC cell lines with MELK reduction using shRNAs targeting MELK. The expression of MELK in NPC cells was reduced in response to three shRNAs targeting MELK (sh-MELK 1#: 0.54±0.03 and 0.68±0.04, sh-MELK 3#: 0.57±0.04 and 0.62±0.03), and the sh-MELK 2#-infected cells with the most significant differences (0.39±0.03 and 0.46±0.02) were used for subsequent experiments (Fig. 2A). The results of the colony formation assay showed that the proliferation of NPC cells was reduced after MELK downregulation (from 206.00±24.56 and 144.00±12.00 to 154.33±7.57 and 104.00±10.82) (Fig. 2B). Transwell assays demonstrated that sh-MELK repressed cell migration (from 296.67±42.00 and 217.33±16.65 to 195.00±20.52 and 154.00±14.18) and invasion (from 236.67±16.04 and 143.00±14.00 to 151.67±15.50 and 108.00±16.09) (Fig. 2C). A positive correlation between the expression of MELK and the immune escape-related factor PD-L1 (CD274) was queried in GEPIA (Fig. 2D). We, therefore, measured the expression of PD-L1 in NPC cells. The downregulation of MELK decreased the expression of PD-L1 (from 0.77±0.03 and 0.75±0.12 to 0.50±0.03 and 0.43±0.05) (Fig. 2E).

MELK downregulation enhances $CD8^+$ T cell-mediated anti-tumor immunity

NPC cells with different infections were co-cultured with sorted $CD8^+$ cells. NPC cells and cell culture supernatants were collected at the end of the co-culture. Flow cytometry was used to evaluate the cancer cell-killing effect of $CD8^+$ T cells. The NPC cells in the sh-MELK group (the apoptosis rate of HNE3 and C666-1 were: 24.24±1.63 and 26.45±1.34) were more sensitive to the killing effect of $CD8^+$ T cells compared with the sh-NC treatment (the apoptosis rate of HNE3 and C666-1 were: 13.40±2.17 and 14.64±1.26) (Fig. 3A). In addition, we also examined Perforin, Granzyme B, IFN-γ, IL-2, and TNF-α secreted by $CD8^+$ T cells in the supernatant of cell co-cultures. ELISA results showed that downregulation of MELK increased Perforin (75.45±4.58 and 86.28±5.48 to 123.28±7.22 and 155.12±8.84), Granzyme B (54.42±3.60 and 67.75±4.12 to 98.23±5.89 and 109.54±8.31), IFN-γ (104.74±17.51 and 135.23±11.13 to 197.33±25.03 and 228.69±29.30), IL-2 (117.15±14.15 and 145.40±18.23 to 246.98±35.20 and 291.59±42.49), and TNF-α (74.22±8.57 and 107.20±2.56 to 182.52±24.12,193.48±21.15) secretion by $CD8^+$ T cells (Fig. 3B).

HNE3 cells after different infections were injected into nude mice to develop *in vivo* models and tumor burden was measured at an interval of 5 d. MELK downregulation in NPC cells significantly reduced tumor growth in mice. At the endpoint, tumor volume in the sh-NC group was 627.49±92.35 mm^3, while the tumor volume of mice in the sh-MELK group decreased to 422.73±67.34 mm^3 (Fig. 3C). In terms of tumor weight, sh-MELK contributed to a decline from 0.59±0.08 g to 0.38±0.04 g (Fig. 3D). T lymphocytes were collected from mouse tumor tissues, and infiltration of $CD8^+$ T cells in mouse tumor tissues was detected by flow cytometry. MELK downregulation increased the infiltration of $CD8^+$ T cells (from 19.57±1.89% to

33.07±3.38%) in tumor tissues (Fig. 3E). In addition, the proportion of IFN-γ$^+$ cells was increased (from 8.72±0.95% to 13.10±1.64%) in CD8$^+$ T cells, suggesting that MELK downregulation further activated CD8$^+$ T cells (Fig. 3F). In addition, we analyzed the number of CD4$^+$ T cells as well as Treg cells in tumor tissues and showed that the percentage of CD4$^+$ T cells in tumor tissues decreased after downregulation of MELK (from 57.23±9.65% to 42.20±5.67%) (Fig. 3G). An increased percentage of Treg cells (CD25$^+$Foxp3$^+$) was observed in tumor tissue (from 13.31±1.42% to 19.75±2.44%) (Fig. 3H).

EP300 synergizes with E2F1 to regulate the MELK promoter

We downloaded the upstream transcription factors of MELK in hTFtarget. The top 20 transcription factors were subjected to intersection analysis in String. EP300 and E2F1 were found to be the core proteins of the PPI network (Fig. 4A). Western blot results showed that EP300 and E2F1 were highly expressed in HNE3 (0.64±0.04 and 0.72±0.06) and C666-1 cells (0.41±0.03 and 0.50±0.04) relative to NP69 cells (0.34±0.01 and 0.37±0.04) (Fig. 4B). A query in hTFtarget revealed a

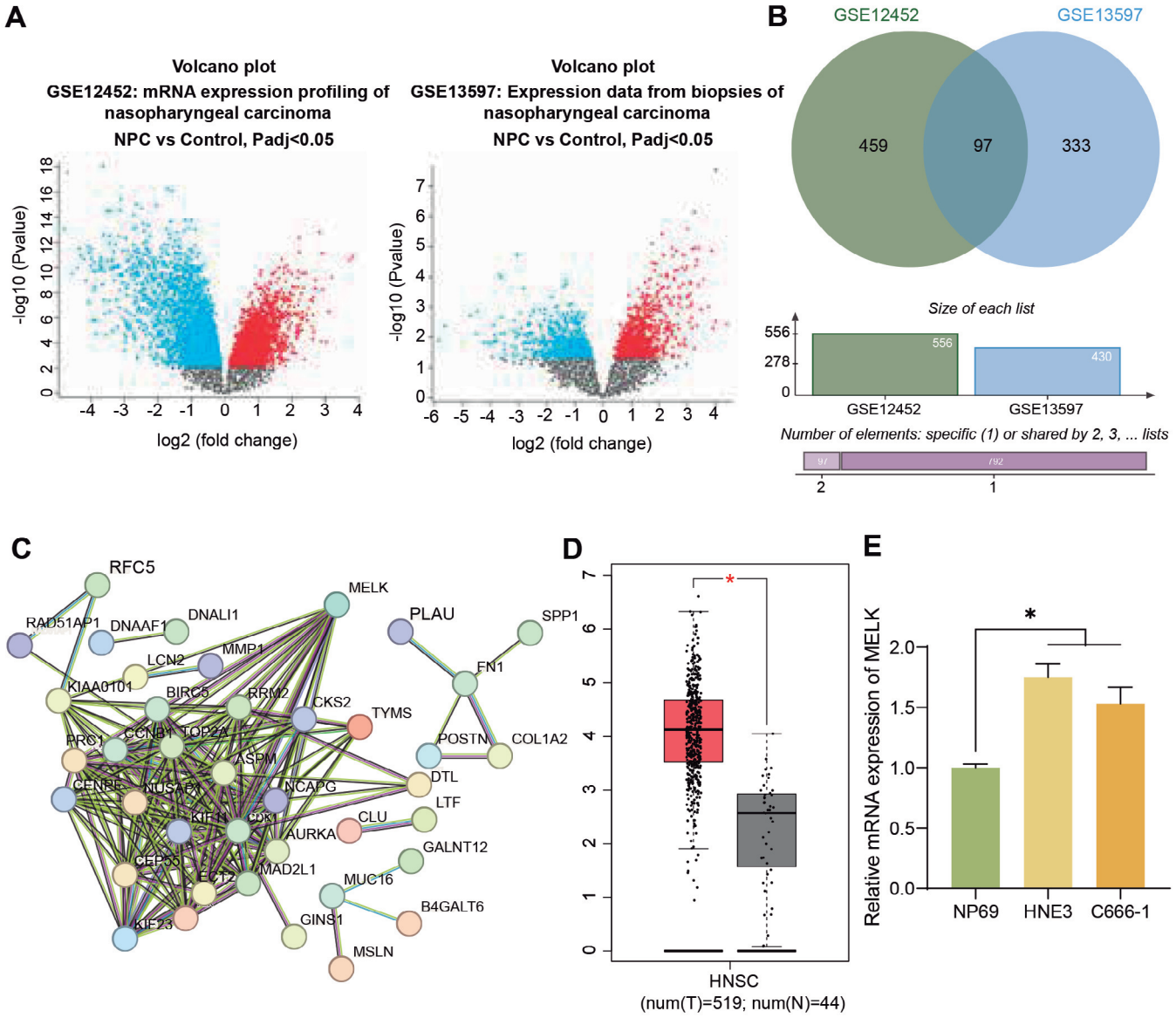

Fig. 1. MELK is overexpressed in NPC. **A.** Volcano maps of differentially expressed genes in the GSE12452 and GSE13597 datasets. **B.** Intersection of differentially expressed genes in the GSE12452 and GSE13597 datasets. **C.** PPI networks of intersection factors in the GSE12452 and GSE13597 datasets. **D.** Expression of MELK in HNSC patients (n=519) and normal controls (n=44) on the GEPIA website. **E.** Detection of MELK expression in nasopharyngeal epithelial cells and NPC cells by RT-qPCR. Values are means±SD, n=3, *p<0.05 (one-way ANOVA).

binding relationship between EP300/E2F1 and MELK promoter (Fig. 4C). Furthermore, the presence of the H3K27Ac histone modification site at the binding of the MELK promoter was shown by the UCSC database (https://genome.ucsc.edu/) (Fig. 4D). ChIP-qPCR results showed that in HNE3 cells, the enrichment of the MELK promoter in the complexes pulled down by antibodies to EP300, E2F1, and H3K27Ac was 9.34±0.53, 12.29±0.62, and 21.59±1.17 relative to IgG antibody, respectively. In C666-1 cells, the enrichment of the MELK promoter in the complexes pulled down by antibodies to EP300, E2F1, and H3K27Ac was 7.82±0.41, 9.13±0.50, and 16.26±0.82 relative to IgG antibody, respectively (Fig. 4E). The results of the dual luciferase assay showed that transfection of EP300 overexpression plasmid resulted in increased MELK-WT luciferase activity (1.84±0.07), which was decreased after sh-E2F1 transfection (1.15±0.05). In contrast, transfection of oe-EP300 (1.06±0.05) and sh-E2F1 (0.94±0.04) did not affect the MELK-MUT (Fig. 4F).

EP300 or E2F1 downregulation suppresses NPC cell activity and immune escape

RT-qPCR was used to determine the expression of EP300 and E2F1 in HNE3 and C666-1 cells after EP300

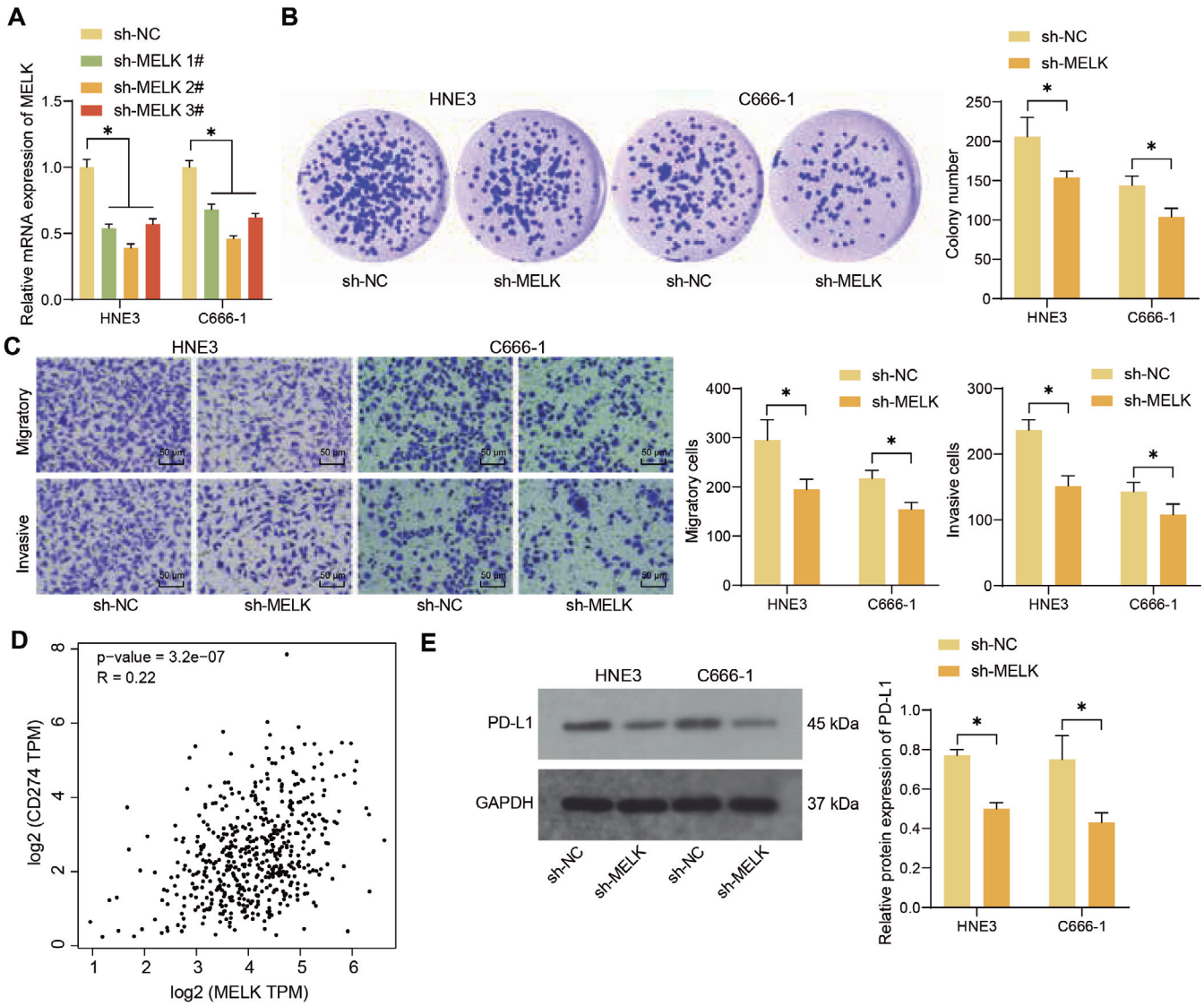

Fig. 2. MELK knockdown suppresses the malignant phenotype of NPC and modulates PD-L1 expression. NPC cells with MELK downregulation were developed by lentiviral infection. **A.** Detection of MELK expression in NPC cells by RT-qPCR. **B.** The clonogenic ability of cells was measured using a colony formation assay. **C.** Cell migration and invasion were measured using Transwell assays. **D.** Correlation of MELK and PD-L1 queried in GEPIA. **E.** PD-L1 protein expression in NPC cells was measured using western blot analyses. Values are means±SD, n=3, *p<0.05 (two-way ANOVA).

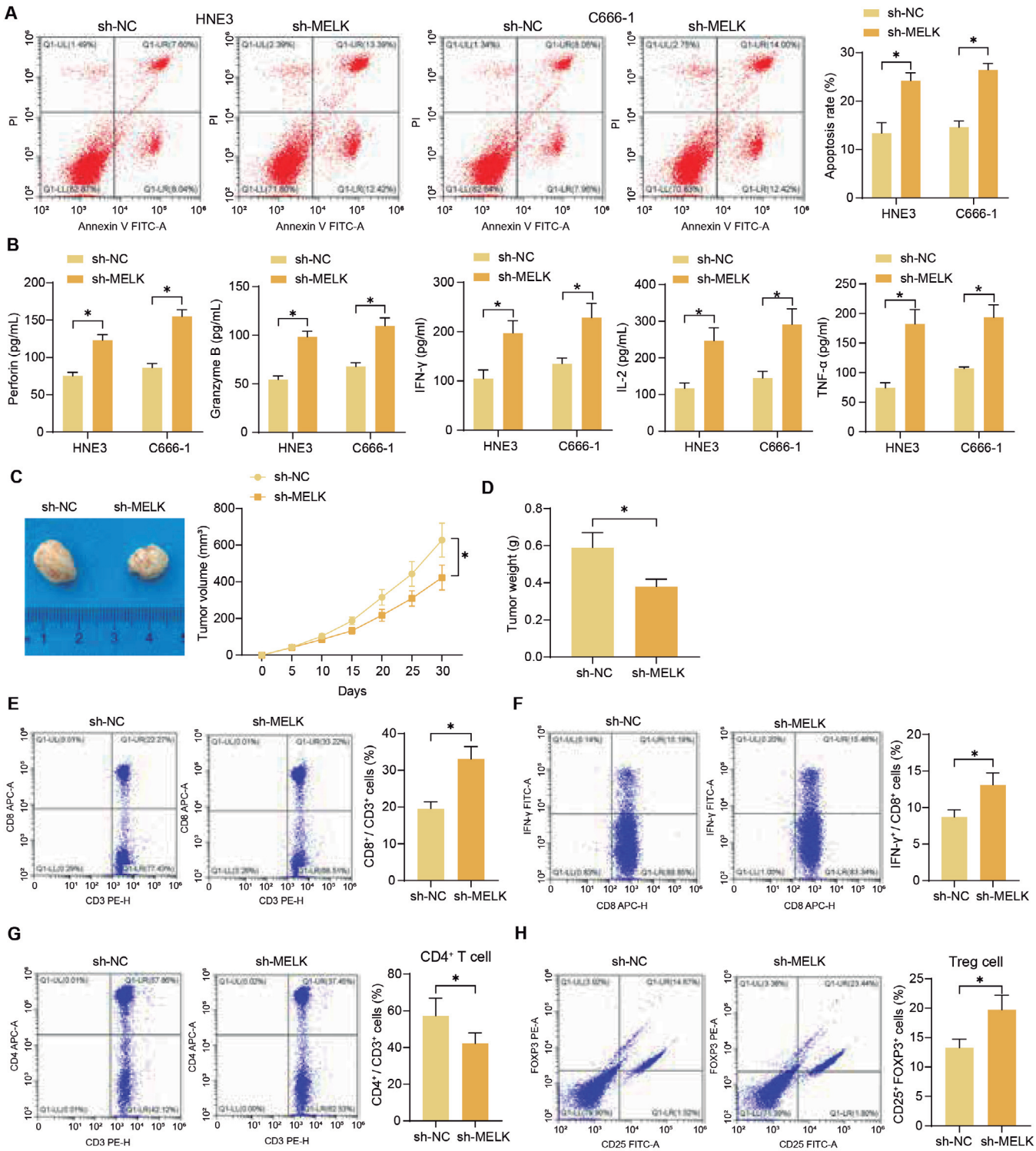

Fig. 3. MELK downregulation mediates the cytotoxicity of CD8⁺ T cells. Activated CD8⁺ cells were co-cultured with NPC cells. **A.** Apoptosis of NPC cells in the co-culture system was measured using flow cytometry. **B.** Perforin, Granzyme B, IFN-γ, IL-2, and TNF-α levels in the cell culture supernatant were measured using ELISA. HNE3 cells were injected subcutaneously into the abdomen of mice, and the volume of tumor tissue **(C)** and the weight of the tumor **(D)** were measured. The ratio of CD8⁺/CD3⁺ T cells **(E)** and IFN-γ⁺/CD8⁺ T cells **(F)**, CD3⁺/CD4⁺ T cells **(G)**, and CD25⁺Foxp3⁺ **(H)** in tumor tissues of mice measured using flow cytometry. Values are means±SD, n=3 (A-B) or 5 (C-H), *p<0.05 (unpaired t-test or two-way ANOVA).

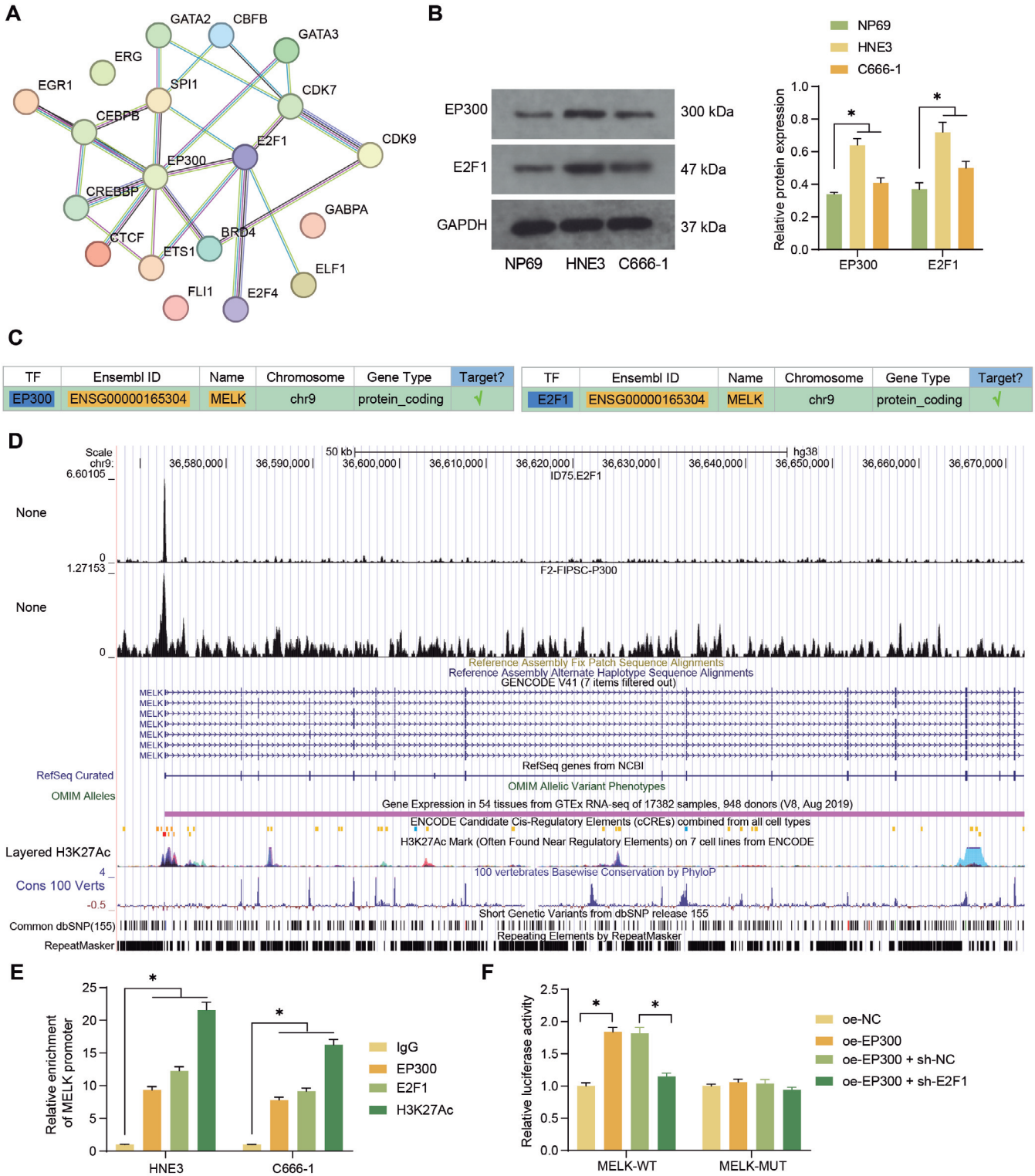

Fig. 4. EP300/E2F1 promotes the transcriptional activity of MELK. **A.** PPI network diagram of the upstream transcriptional factors of MELK analyzed by String. **B.** EP300 and E2F1 expression in NPC cells were measured using western blot analyses. **C.** Transcriptional regulation of MELK by EP300/E2F1 queried by hTFtarget. **D.** Binding peaks of EP300, E2F1, and H3K27Ac on the MELK promoter queried in the UCSC database. **E.** The binding relationship between EP300, E2F1, H3K27Ac, and MELK promoter using ChIP-qPCR. **F.** The transcriptional activity of MELK in response to EP300 overexpression and E2F1 downregulation using dual-luciferase assay. Values are means±SD, n=3, *p<0.05 (two-way ANOVA).

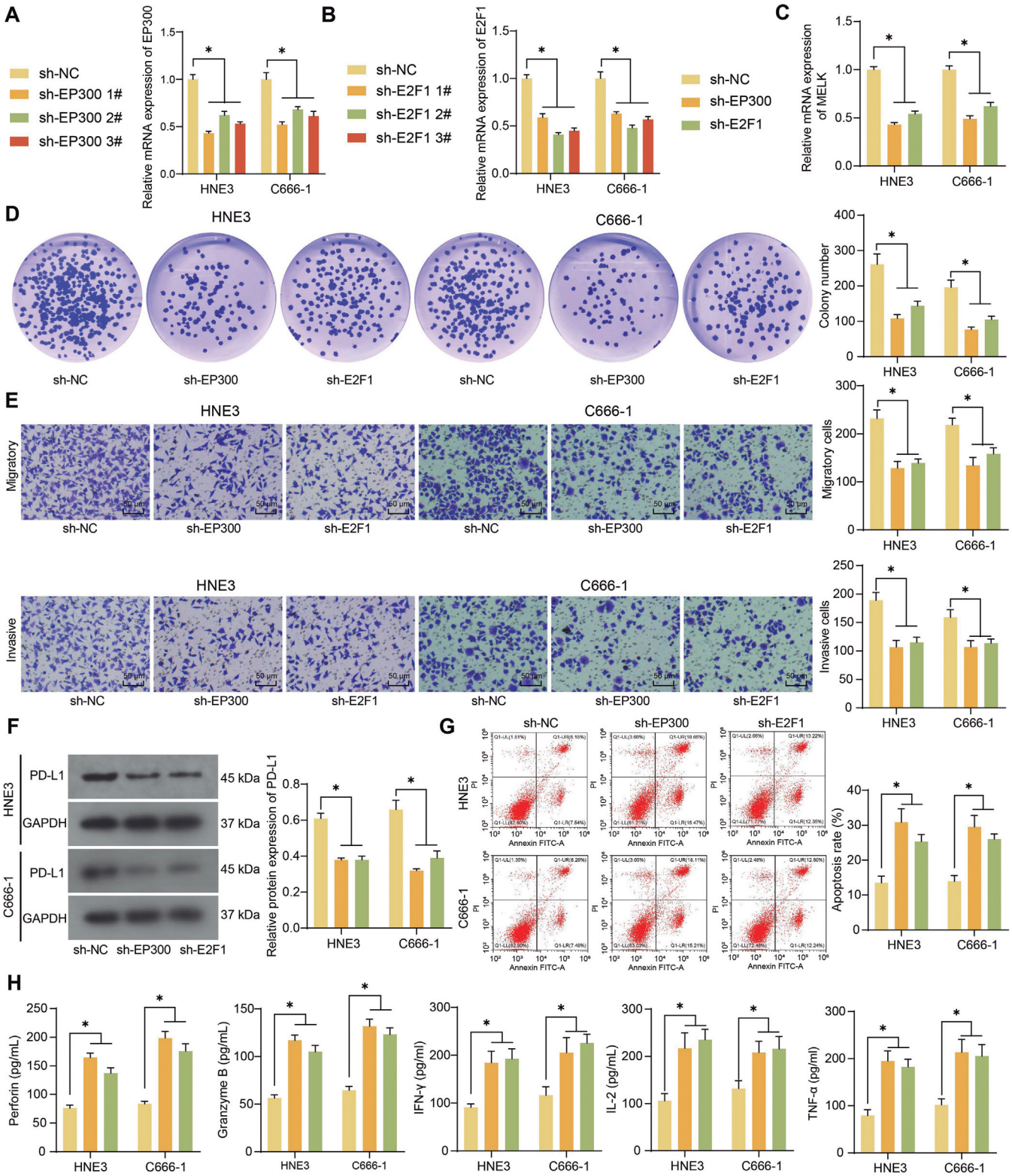

Fig. 5. Downregulation of EP300 or E2F1 reverts the malignant phenotype of NPC cells and promotes the cytotoxicity of $CD8^+$ T cells. NPC cell lines with EP300 or E2F1 downregulation were developed by lentiviral infection. EP300 **(A)**, E2F1 **(B)**, and MELK **(C)** expression in NPC cell lines using RT-qPCR assays. **D.** The clonogenic ability of cells was measured using a colony formation assay. **E.** Cell migration and invasion were measured using Transwell assays. **F.** PD-L1 protein expression in NPC cells was measured using western blot analyses. Activated $CD8^+$ cells were co-cultured with NPC cells. **G.** Apoptosis of NPC cells in the co-culture system was measured using flow cytometry. **H.** Perforin, Granzyme B, IFN-γ, IL-2, and TNF-α levels in the cell culture supernatant were measured using ELISA. Values are means±SD, n=3, *p<0.05 (two-way ANOVA).

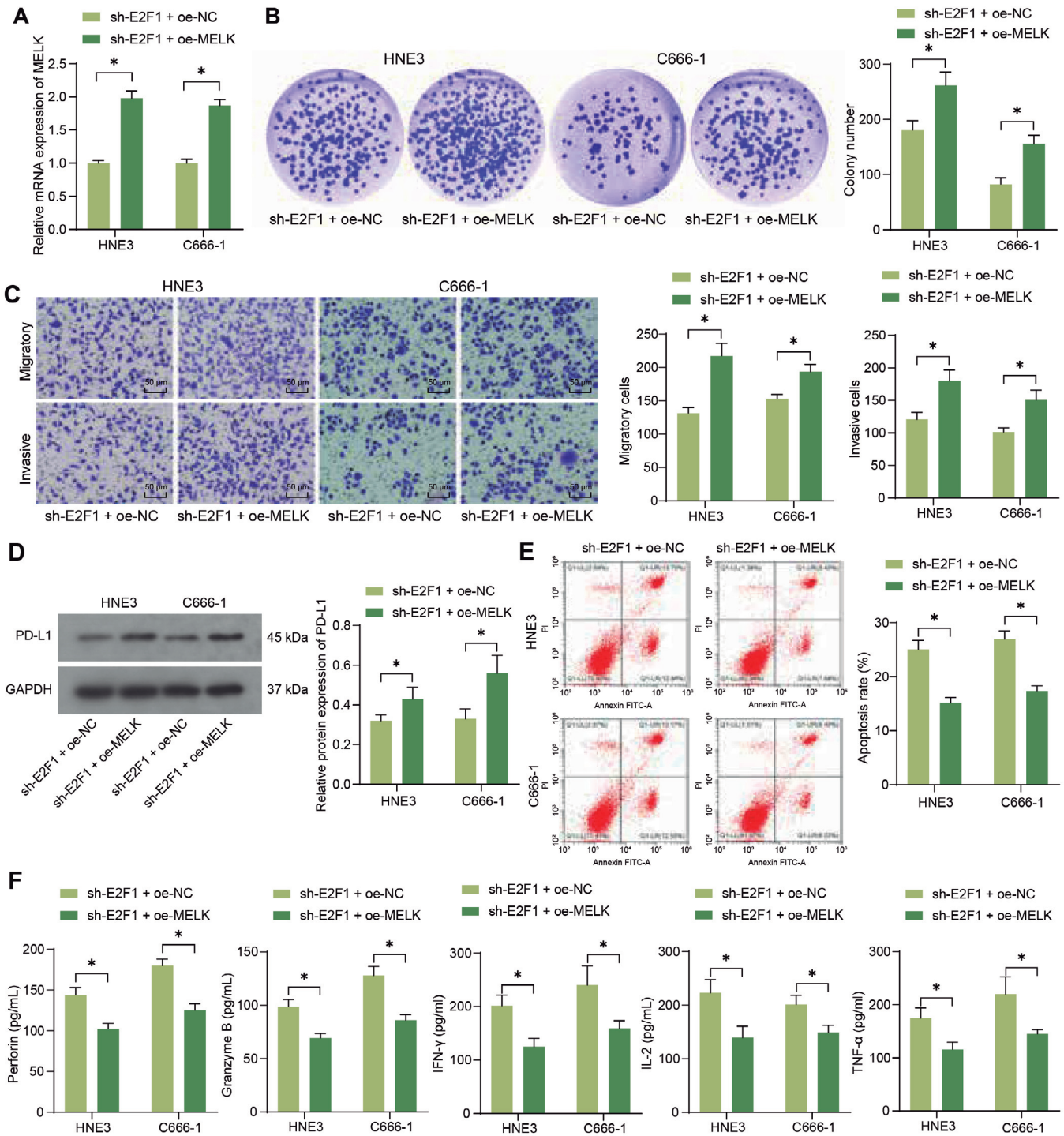

Fig. 6. E2F1 mediates CD8$^+$ T cells through MELK. NPC cell lines with sh-E2F1 were further infected with MELK overexpression. **A.** MELK expression in NPC cell lines using RT-qPCR assays. **B.** The clonogenic ability of cells was measured using a colony formation assay. **C.** Cell migration and invasion were measured using Transwell assays. **D.** PD-L1 protein expression in NPC cells was measured using western blot analyses. Activated CD8$^+$ cells were co-cultured with NPC cells infected with sh-E2F1 + oe-MELK or sh-E2F1 + oe-NC. **E.** Apoptosis of NPC cells in the co-culture system was measured using flow cytometry. **F.** Perforin, Granzyme B, IFN-γ, IL-2, and TNF-α levels in the cell culture supernatant were measured using ELISA. Values are means±SD, n=3, *p<0.05 (two-way ANOVA).

or E2F1 downregulation with shRNAs (Fig. 5A,B). The sh-EP300 1# (sh-EP300 1#: 0.43±0.02 and 0.52±0.03, sh-EP300 2#: 0.62±0.04 and 0.68±0.03, sh-EP300 3#: 0.53±0.02 and 0.61±0.05) and sh-E2F1 2# (sh-E2F1 1#: 0.59±0.04 and 0.63±0.02, sh-E2F1 2#: 0.41±0.02 and 0.48±0.03, sh-E2F1 3#: 0.45±0.03 and 0.57±0.03) were selected for the subsequent experiments. In addition, RT-qPCR results indicated that the relative mRNA expression of MELK in HNE3 and C666-1 cells was reduced to 0.43±0.02 and 0.49±0.03 in the presence of sh-EP300, and 0.54±0.03 and 0.62±0.04 in the presence of sh-E2F1 (Fig. 5C). The number of colonies formed by HNE3 and C666-1 decreased from 261.33±29.09 and 196.33±20.21 to 108.00±11.14 and 76.67±7.09 after the downregulation of EP300. Similarly, the number of colonies formed by HNE3 and C666-1 decreased to 143.67±13.58 and 105.33±9.29 after the downregulation of E2F1 (Fig. 5D). In addition, the number of migrated cells decreased from 232.00±17.58 and 218.67±13.87 to 128.67±14.01 and 134.33±16.56 after downregulation of EP300, respectively, and the number of migrated cells decreased to 139.33±8.33 and 158.33±12.50 after downregulation of E2F1. Consistently the number of invaded cells decreased from 189.00±13.75 and 159.00±13.53 to 106.67±11.93 and 107.00±11.14 after the downregulation of EP300, respectively, the number of invaded cells decreased to 115.00±9.17 and 113.67±7.51 after downregulation of E2F1 (Fig. 5E). Western blot results showed that the basal expression of PD-L1 was 0.61±0.03 and 0.66±0.05, which was further reduced by sh-EP300 (0.38±0.01 and 0.32±0.01) or sh-E2F1 (0.38±0.02 and 0.39±0.04) in NPC cells (Fig. 5F). Decreased expression of EP300 or E2F1 in NPC cells, on the contrary, increased the killing effects of CD8+ T cells on NPC cells, leading to an increased apoptosis rate (30.89±3.85% and 29.54±3.28% for sh-EP300 and 25.36±2.00% and 26.04±1.47% for sh-E2F1) (Fig. 5G). ELISA results showed elevated Perforin (164.45±7.86 and 198.45±11.95 for sh-EP300; 137.28±9.25 and 175.78±12.71 for sh-E2F1), Granzyme B (116.92±5.56 and 131.80±7.36 for sh-EP300; 105.01±6.68 and 123.23±6.79 for sh-E2F1), IFN-γ (184.49±23.98 and 205.60±31.27 for sh-EP300; 192.64±21.07 and 225.73±18.28 for sh-E2F1), IL-2 (217.14±32.86 and 208.25±23.95 for sh-EP300; 235.40±21.85 and 216.19±25.85 for sh-E2F1), and TNF-α (195.11±21.35 and 213.69±27.04 for sh-EP300; 182.55±16.28 and 205.28±24.56 for sh-E2F1) levels in the co-culture system (Fig. 5H).

MELK overexpression reverses the suppression of immune escape by E2F1 downregulation

To verify the promoting role of E2F1 on MELK transcription in NPC, we further treated sh-E2F1-infected NPC cells with oe-MELK. The mRNA expression of MELK was elevated to 1.98±0.11 and 1.87±0.09 in NPC cells after lentivirus infection (Fig. 6A). Compared to cells in the sh-E2F1 + oe-NC group, NPC cells in the sh-E2F1 + oe-MELK group showed an increased number of colonies formed (261.67±24.03 and 155.67±15.50) (Fig. 6B). The observations derived from Transwell assays demonstrated that the number of migrated (from 131.33±8.74 and 153.00±6.56 to 217.33±18.72 and 193.67±11.06) and invaded (from 120.67±11.15 and 101.33±6.51 to 180.00±16.70 and 151.00±14.93) cells was promoted after MELK overexpression (Fig. 6C). MELK overexpression upregulated PD-L1 expression (0.43±0.06 and 0.56±0.09) in NPC cells (Fig. 6D). Furthermore, MELK overexpression suppressed the killing effect of $CD8^+$ T cells on NPC cells, and the apoptosis rate decreased to 15.18±0.97% and 17.40±0.93% (Fig. 6E) and suppressed the secretion of Perforin (102.62±6.43 and 125.45±7.81), Granzyme B (69.42±4.26 and 85.96±5.26), IFN-γ (125.11±15.41 and 159.31±14.29), IL-2 (139.52±21.16 and 149.37±12.89), and TNF-α (116.03±13.53 and 145.25±8.18) levels by $CD8^+$ T cells (Fig. 6F).

Discussion

The Ser/Thr protein kinase MELK has been regarded as a promising therapeutic target for cancer management since 2005 (McDonald and Graves, 2020). However, little research drew the connection between MELK and immune escape, a hotspot in cancer research. We demonstrated that MELK plays a modulating role in the $CD8^+$ T response directed against NPC cells, probably via a reduction of PD-L1 expression. Additionally, the E2F1-EP300 co-activator complex might be responsible for the upregulation of MELK in NPC.

MELK overexpression was related to higher histological grade, advanced clinical stage, and compromised overall survival in patients with endometrial carcinoma and ovarian cancer (Kohler et al., 2017; Xu et al., 2020), indicating the possible prognostic role of MELK. As for its functional role, the knockdown of MELK repressed the migration and invasion of lung adenocarcinoma cells (Tang et al., 2020). More importantly, MELK accelerated tumor growth and lung metastases, whereas the knockdown of MELK in esophageal squamous cell carcinoma cells contributed to the opposite effect (Chen et al., 2020). Apart from that, cell proliferation, derived from the mean expression of 10 proliferation-associated genes, including MELK, was identified as a marker of response to immune checkpoint inhibitors in non-small cell lung cancer (Pabla et al., 2019), suggesting its connection with immune response. In this study, we not only observed the suppressing effects of sh-MELK on the colony formation, migration, and invasion of cells but also verified the positive correlation between MELK and PD-L1 expression. Cytotoxic $CD8^+$ T cells are a major subset of immune cells that clear tumor cells, and they need to be activated first and then hone to the tumor site to stimulate an efficient immune response (Jiang et al., 2020). $CD8^+$ T

cells are capable of killing cells by releasing cytotoxic molecules, such as granzymes and perforin, into the immunological synapse and secrete cytokines, such as IFN-γ, TNF-α, and IL-2 (Mittrucker et al., 2014). Here, we found that the NPC cells with knockdown of MELK were more sensitive to activated $CD8^+$ T cells, as evidenced by enhanced NPC cell apoptosis and enhanced Perforin, Granzyme B, IFN-γ, TNF-α, and IL-2 levels in the co-culture system. Our *in vivo* findings also demonstrated that nude mice with sh-MELK had reduced tumor burden and enhanced $CD8^+$ T infiltration.

Regarding the upstream mechanism for the upregulation of MELK, it has been described that a long noncoding RNA BBOX1-AS1 contributed to cell malignant phenotypes in non-small cell lung cancer by interacting with microRNA-27a-5p to upregulate MELK (Shi et al., 2021). Intriguingly, the oncogenic role of MELK in cervical cancer has been associated with E2F1 (Sun et al., 2021). Furthermore, Ropolo et al. found that the E2F1-EP300 co-activator complex was a part of the regulatory pathway controlling the promoter activity of vacuole membrane protein 1 triggered by gemcitabine in pancreatic cancer cells (Ropolo et al., 2020). In the same vein, we identified both EP300 and E2F1 as the upstream transcription factors of MELK in the present study. It has been revealed by Sheikh et al. that the histone acetyltransferase MOZ is required to maintain normal levels of H3K27 acetylation at the transcriptional start sites of MELK (Sheikh et al., 2015), indicating the possible interaction between MELK transcription and the H3K27 acetylation. We also observed the enrichment of the MELK promoter in the complex immunoprecipitated by antibodies of EP300, E2F1, and H3K27Ac. We substantiated the enhanced effects of sh-EP300 and sh-E2F1 on the antitumor immune responses in NPC. Downregulation of EP300 was associated with higher antitumor immunity in most solid malignancies (Krupar et al., 2020). E2F1 rendered prostate cancer cells resistant to the antitumor immunity mediated by ICAM-1, another molecule capable of enhancing T-cell ability to kill targets (Ren et al., 2014). However, to the best of our knowledge, many questions remain untouched and unanswered regarding the immunomodulation of EP300 and E2F1 in NPC. We observed that overexpression of MELK reversed the effects of sh-E2F1 on both the aggressiveness of NPC cells and the cytotoxicity of $CD8^+$ T cells, which further suggested that MELK was the downstream effector of E2F1 in modulating the antitumor immunity in NPC.

There are certain limitations in the current study. First, C57BL/6J mice with intact immune activity were used in the *in vivo* study, and humanized mice that can better mimic the human immune characteristics should be used to support our conclusion. In addition, since the fixation of the cell and the blocking of the secretion of IFN-γ was neglected in the flow cytometry during the assessment of IFN-γ, the result of flow cytometry may cause some error.

In conclusion, EP300-E2F1 is a negative modulator of antitumor immune responses in NPC via the inactivation of $CD8^+$ T cells through MELK. MELK blockade may enhance the sensitivity of NPC cells to $CD8^+$ T cell-mediated anti-tumor immune response.

Funding. None.
Conflict of interest. There is no conflict of interest.

References

Baloche V., Ferrand F.R., Makowska A., Even C., Kontny U. and Busson P. (2020). Emerging therapeutic targets for nasopharyngeal carcinoma: Opportunities and challenges. Expert Opin. Ther. Targets. 24, 545-558.

Chan O.S., Kowanetz M., Ng W.T., Koeppen H., Chan L.K., Yeung R.M., Wu H., Amler L. and Mancao C. (2017). Characterization of PD-L1 expression and immune cell infiltration in nasopharyngeal cancer. Oral Oncol. 67, 52-60.

Chen Y.P., Chan A.T.C., Le Q.T., Blanchard P., Sun Y. and Ma J. (2019). Nasopharyngeal carcinoma. Lancet 394, 64-80.

Chen L., Wei Q., Bi S. and Xie S. (2020). Maternal embryonic leucine zipper kinase promotes tumor growth and metastasis via stimulating foxm1 signaling in esophageal squamous cell carcinoma. Front. Oncol. 10, 10.

Gong L., Kwong D.L., Dai W., Wu P., Wang Y., Lee A.W. and Guan X.Y. (2021). The stromal and immune landscape of nasopharyngeal carcinoma and its implications for precision medicine targeting the tumor microenvironment. Front. Oncol. 11, 744889.

Jiang W., He Y., He W., Wu G., Zhou X., Sheng Q., Zhong W., Lu Y., Ding Y., Lu Q., Ye F. and Hua H. (2020). Exhausted cd8+t cells in the tumor immune microenvironment: New pathways to therapy. Front. Immunol. 11, 622509.

Kohler R.S., Kettelhack H., Knipprath-Meszaros A.M., Fedier A., Schoetzau A., Jacob F. and Heinzelmann-Schwarz V. (2017). MELK expression in ovarian cancer correlates with poor outcome and its inhibition by OTSSP167 abrogates proliferation and viability of ovarian cancer cells. Gynecol. Oncol. 145, 159-166.

Krupar R., Watermann C., Idel C., Ribbat-Idel J., Offermann A., Pasternack H., Kirfel J., Sikora A.G. and Perner S. (2020). In silico analysis reveals EP300 as a pancancer inhibitor of anti-tumor immune response via metabolic modulation. Sci. Rep. 10, 9389.

Lee A.W., Ma B.B., Ng W.T. and Chan A.T. (2015). Management of nasopharyngeal carcinoma: Current practice and future perspective. J. Clin. Oncol. 33, 3356-3364.

Li B., Xu X., Bin X., Zhou J. and Tang Z. (2021). Ectopic expression of MELK in oral squamous cell carcinoma and its correlation with epithelial mesenchymal transition. Aging (Albany NY). 13, 13048-13060.

Li Y., Dong H., Dong Y., Wu Q., Jiang N., Luo Q. and Chen F. (2022). Distribution of CD8 T cells and NK cells in the stroma in relation to recurrence or metastasis of nasopharyngeal carcinoma. Cancer Manag. Res. 14, 2913-2926.

McDonald I.M. and Graves L.M. (2020). Enigmatic MELK: The controversy surrounding its complex role in cancer. J. Biol. Chem. 295, 8195-8203.

Mittrucker H.W., Visekruna A. and Huber M. (2014). Heterogeneity in the differentiation and function of $CD8^+$ T cells. Arch. Immunol. Ther. Exp. (Warsz). 62, 449-458.

Oshi M., Gandhi S., Huyser M.R., Tokumaru Y., Yan L., Yamada A.,

Matsuyama R., Endo I. and Takabe K. (2021). MELK expression in breast cancer is associated with infiltration of immune cell and pathological compete response (pCR) after neoadjuvant chemotherapy. Am. J. Cancer Res. 11, 4421-4437.

Pabla S., Conroy J.M., Nesline M.K., Glenn S.T., Papanicolau-Sengos A., Burgher B., Hagen J., Giamo V., Andreas J., Lenzo F.L., Yirong W., Dy G.K., Yau E., Early A., Chen H., Bshara W., Madden K.G., Shirai K., Dragnev K., Tafe L.J., Marin D., Zhu J., Clarke J., Labriola M., McCall S., Zhang T., Zibelman M., Ghatalia P., Araujo-Fernandez I., Singavi A., George B., MacKinnon A.C., Thompson J., Singh R., Jacob R., Dressler L., Steciuk M., Binns O., Kasuganti D., Shah N., Ernstoff M., Odunsi K., Kurzrock R., Gardner M., Galluzzi L. and Morrison C. (2019). Proliferative potential and resistance to immune checkpoint blockade in lung cancer patients. J. Immunother. Cancer 7, 27.

Ren Z., Kang W., Wang L., Sun B., Ma J., Zheng C., Sun J., Tian Z., Yang X. and Xiao W. (2014). E2F1 renders prostate cancer cell resistant to ICAM-1 mediated antitumor immunity by NF-κB modulation. Mol. Cancer 13, 84.

Ropolo A., Catrinacio C., Renna F.J., Boggio V., Orquera T., Gonzalez C.D. and Vaccaro M.I. (2020). A novel E2F1-EP300-VMP1 pathway mediates gemcitabine-induced autophagy in pancreatic cancer cells carrying oncogenic KRAS. Front. Endocrinol. 11, 411.

Sheikh B.N., Phipson B., El-Saafin F., Vanyai H.K., Downer N.L., Bird M.J., Kueh A.J., May R.E., Smyth G.K., Voss A.K. and Thomas T. (2015). MOZ (MYST3, KAT6A) inhibits senescence via the INK4A-ARF pathway. Oncogene 34, 5807-5820.

Shi J., Yang C., An J., Hao D., Liu C., Liu J., Sun J. and Jiang J. (2021). KLF5-induced BBOX1-AS1 contributes to cell malignant phenotypes in non-small cell lung cancer via sponging miR-27a-5p to up-regulate MELK and activate FAK signaling pathway. J. Exp. Clin. Cancer Res. 40, 148.

Sun H., Ma H., Zhang H. and Ji M. (2021). Up-regulation of MELK by E2F1 promotes the proliferation in cervical cancer cells. Int. J. Biol. Sci. 17, 3875-3888.

Sung H., Ferlay J., Siegel R.L., Laversanne M., Soerjomataram I., Jemal A. and Bray F. (2021). Global cancer statistics 2020: GLOBOCAN estimates of incidence and mortality worldwide for 36 cancers in 185 countries. CA Cancer J. Clin. 71, 209-249.

Tang Q., Li W., Zheng X., Ren L., Liu J., Li S., Wang J. and Du G. (2020). MELK is an oncogenic kinase essential for metastasis, mitotic progression, and programmed death in lung carcinoma. Signal Transduct. Target. Ther 5, 279.

Thangaraj K., Ponnusamy L., Natarajan S.R. and Manoharan R. (2020). MELK/MPK38 in cancer: From mechanistic aspects to therapeutic strategies. Drug Discov. Today 25, 2161-2173.

Xiao Y. and Yu D. (2021). Tumor microenvironment as a therapeutic target in cancer. Pharmacol. Ther. 221, 107753.

Xu Q., Ge Q., Zhou Y., Yang B., Yang Q., Jiang S., Jiang R., Ai Z., Zhang Z. and Teng Y. (2020). MELK promotes endometrial carcinoma progression via activating mTOR signaling pathway. EBioMedicine 51, 102609.

Accepted September 6, 2023